Two-center convergent close-coupling approach to positron–helium-ion collisions

C. M. Rawlins, A. S. Kadyrov, and I. Bray
Curtin Institute for Computation and Department of Physics, Astronomy and Medical Radiation Sciences, Curtin University, GPO Box U1987, Perth, Western Australia 6845, Australia

(Received 7 December 2017; published 30 January 2018)

We generalize the two-center convergent close-coupling approach of Kadyrov and Bray [Phys. Rev. A **66**, 012710 (2002)] for positron scattering on neutral targets to charged targets, and apply it to positron scattering on the singly charged helium ion. Where possible internal consistency checks are used to validate the two-center method, which required a significant redevelopment of the positronium-formation matrix elements, by comparison with a single-center approach. Only the two-center approach explicitly yields positronium formation, and so it also provides a mechanism to calculate positronium scattering on α particles. As yet there are no experiments for the calculated processes, but there are some previous theoretical calculations, with which comparison is mixed.

DOI: 10.1103/PhysRevA.97.012707

I. INTRODUCTION

Collision systems involving positrons incident on ions have attracted less attention than those involving neutral targets [1]. In a simple one-center approach to positron scattering, where the total wave function is expanded in just the target states, the transition from a neutral target to a charged one is relatively straightforward, involving the replacement of the spherical Bessel functions used to describe the projectile partial waves by Coulomb functions [2]. However, one-center approaches cannot explicitly calculate positronium (Ps) formation, or the reverse process of (anti)hydrogen formation upon Ps scattering on (anti)protons [1]. For such calculations two-center approaches, which explicitly incorporate charge exchange to form positronium, are necessary.

Two-center approaches to positron-atom scattering are much more complicated than the corresponding one-center approaches. This can be seen from the original (one-center) implementation of the convergent close-coupling (CCC) method for electron/positron-hydrogen scattering [3] and the two-center positron-hydrogen CCC implementation [4]. The extra center requires the usage of different coordinate systems, and is the primary source of the extra complexity. Consequently, the extension of two-center collision systems to ionic targets is far from being as straightforward as for one-center systems. The simplest ionic target, which is a natural extension from atomic hydrogen, is the positive singly charged helium ion. Here we present the CCC formalism for a two-center approach to calculating $e^+ + \mathrm{He}^+$. The explicit inclusion of Ps formation means that we are then also able to calculate the time-reversed collision system of Ps scattering on α particles (helium nuclei).

Currently no experimental results are available for the e^+-He^+ collision systems due to difficulties associated with He^+ production. The absence of these results means that little interest has been paid to this problem on the theoretical side too. Nevertheless, variational methods were used for He^+ and other hydrogenlike ions to generate phase shifts in the region where only elastic scattering is possible [5,6]. In addition, between 50 and 300 eV, close-coupling (CC) methods were used to calculate cross sections for various processes for the $e^+ + \mathrm{He}^+$ system [7]. The most recent calculations using 19 He^+ states and 1 Ps state [CC(19,1)] and 26 He^+ states and 3 Ps states [CC(26,3)] were reported in Ref. [8]. While these results provided information on more scattering processes than previous variational calculations, there were some clear discrepancies between the two types of calculations for the phase shifts. Most recently, Ps formation was investigated using a two-center eikonal-final-state continuum-initial-distorted-wave (EFS-CDW) method [9,10]. However, when comparing total Ps formation cross sections with those from the CC calculations, they can differ by as much as 50%. Therefore, accurate calculations are required in order to verify the aforementioned methods in the absence of experimental data.

Initially, the two-center convergent close-coupling (CCC) method was developed for positron scattering on H [4,11]. It was also successfully applied to the calculation of low-energy antihydrogen ($\bar{\mathrm{H}}$) formation cross sections via Ps scattering on antiprotons [12–17]. Later it was extended to include other neutral targets such as helium [18–20], magnesium [21], alkali metals [22–24], and most recently, molecular hydrogen [25]. However, none of these targets have a residual long-range Coulomb interaction in any reaction channel, meaning that the method used in these cases is not applicable to He^+, in particular when Ps formation is included. Thus, the development of an updated two-center CCC method is required to include ionic targets. The calculation and analysis for the first three partial waves ($J = 0$–2) of this system have been reported [26].

For the CCC method, equations for Ps-formation matrix elements involving residual long-range Coulomb interactions are presented in this paper. On the other hand, the direct scattering matrix elements have been used in the CCC method since its inception [2,3,27,28]. The new two-center CCC method that includes Ps-formation channels can be validated against the single-center CCC code via internal consistency checks.

Internal consistency makes use of the completeness of the Laguerre basis to compare single-center CCC calculations with two-center CCC calculations [29]. Below the Ps-formation threshold and above the ionization threshold of the target, both single- and two-center methods should yield the same results for the grand total and electron-loss cross sections. Within these two regions a large enough single-center expansion can be used to account for Ps formation indirectly using positive energy states. Between the Ps($1s$) formation and ionization thresholds (the extended Ore gap), where Ps formation is explicitly required, this idea breaks down due to electron loss not being possible for the single-center approach in this region. Internal consistency has been checked in e^++H and e^++He calculations [29,30]. It is extremely helpful in the present case to access the internal consistency checks as a way of validating the new developments.

The outline of the paper is as follows. The CCC formalism for this problem is given in Sec. II. Details of calculations are given in Sec. III. The results of the calculations, including convergence studies, internal consistency checks, and comparison to previous calculations, are given in Sec. IV. Finally, the main highlights, conclusions, and future directions are given in Sec. V.

II. FORMALISM

A. Basic equations

Consider a system of three particles: positron, electron, and He^{2+} ion. Index α (β) will denote a quantum state in which the positron (He^{2+}) is free and the other two form a bound state and index e will be used for channels where all three particles are free. With this notation the total scattering wave function of the three-body system at a total energy E may be written as

$$(H - E)\Psi = 0, \tag{1}$$

where

$$H = H_0 + v_\alpha + v_\beta + v_e \equiv H_0 + v, \tag{2}$$

and where H_0 is the free-three-particle Hamiltonian and v_i is the Coulomb interaction between particles of pair i ($i = \alpha,\beta,e$).

The Jacobi variable $\boldsymbol{r}_i$ is the relative position of particles in pair i, and $\boldsymbol{\rho}_i$ is the position of the particle i relative to the center of mass (c.m.) of pair i ($i = \alpha,\beta,e$). See Fig. 1. Expanding the total wave function Ψ in terms of the two-body pseudostate wave functions describing the target atom (T) and the Ps subspaces, we write

$$\Psi = \sum_{\alpha=1}^{N^{\rm T}} F_\alpha(\boldsymbol{\rho}_\alpha)\psi_\alpha(\boldsymbol{r}_\alpha) + \sum_{\beta=1}^{N^{\rm Ps}} F_\beta(\boldsymbol{\rho}_\beta)\psi_\beta(\boldsymbol{r}_\beta), \tag{3}$$

where $N^{\rm T}$ ($N^{\rm Ps}$) is the number of pseudostates for the target (Ps) center and ψ_γ ($\boldsymbol{r}_\gamma$) are linear combinations of the complete Laguerre basis functions:

$$\xi_{n,l}^{(\lambda)}(r) = \left(\frac{\lambda(n-1)!}{(2l+1+n)!}\right)^{1/2} \times (\lambda r)^{l+1}\exp[-\lambda r/2]L_{n-1}^{2l+2}(\lambda r). \tag{4}$$

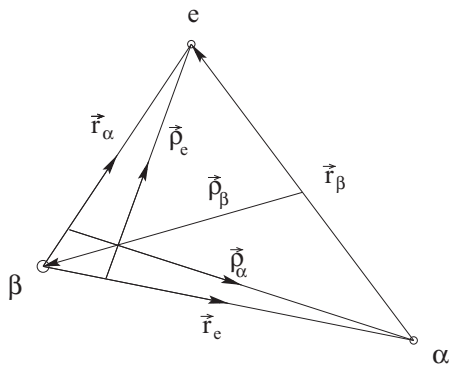

FIG. 1. Jacobi coordinates for the system of three particles: positron (α), He^{2+} ion (β), and electron (e).

Here $L_{n-1}^{2l+2}(x)$ is the associated Laguerre polynomial, and for each angular momentum l, n ranges from 1 to the basis size N_l. These pseudostates diagonalize the two-body Hamiltonian H for both centers:

$$\langle\psi_{\gamma'}|H_\gamma|\psi_\gamma\rangle = \varepsilon_\gamma\delta_{\gamma'\gamma}. \tag{5}$$

Substituting Eq. (3) into Eq. (1) and following [31], we obtain momentum-space coupled-channel equations for transition matrix elements:

$$T_{\gamma',\gamma}(\boldsymbol{q}_{\gamma'},\boldsymbol{q}_\gamma) = V_{\gamma',\gamma}(\boldsymbol{q}_{\gamma'},\boldsymbol{q}_\gamma) + \sum_{\gamma''=1}^{N^{\rm T}+N^{\rm Ps}} \int \frac{d\boldsymbol{q}_{\gamma''}}{(2\pi)^3} \times V_{\gamma',\gamma''}(\boldsymbol{q}_{\gamma'},\boldsymbol{q}_{\gamma''})G_{\gamma''}\left(q_{\gamma''}^2\right)T_{\gamma'',\gamma}(\boldsymbol{q}_{\gamma''},\boldsymbol{q}_\gamma), \tag{6}$$

where $\boldsymbol{q}_\gamma$ is the momentum of free particle γ relative to the c.m. of the bound pair in channel γ. The effective two-body free Green's function is defined as

$$G_{\gamma''}\left(q_{\gamma''}^2\right) = \left[E + i0 - \varepsilon_{\gamma''} - q_{\gamma''}^2/(2M_{\gamma''})\right]^{-1} \tag{7}$$

and describes the free relative motion of particle γ'' and bound pair γ'' with the binding energy $\varepsilon_{\gamma''}$.

The effective potentials are defined as

$$V_{\gamma',\gamma}(\boldsymbol{q}_{\gamma'},\boldsymbol{q}_\gamma) = \langle\boldsymbol{q}_{\gamma'}|\langle\psi_{\gamma'}|U_{\gamma'\gamma}|\psi_\gamma\rangle|\boldsymbol{q}_\gamma\rangle, \tag{8}$$

where

$$U_{\alpha,\alpha} = v - v_\alpha - v_C, \quad U_{\beta,\beta} = v - v_\beta, \quad U_{\alpha,\beta} = U_{\beta,\alpha} = H_0 + v - E \tag{9}$$

are the transition operators. In $U_{\alpha,\alpha}$, the v_C term is the long-range Coulomb interaction between the He^+ ion and the incoming positron.

Upon partial wave expansion in total orbital angular momentum J according to (the same for $T_{\gamma',\gamma}$)

$$V_{\gamma'\gamma}(\boldsymbol{q}_{\gamma'},\boldsymbol{q}_\gamma) = \sum_{L',M',L,M,J,K} Y_{L'M'}(\widehat{\boldsymbol{q}}_{\gamma'})C_{L'M'l'm'}^{JK} \times \mathscr{V}_{\gamma'\gamma}^{L'L}(q_{\gamma'},q_\gamma)C_{LMlm}^{JK}Y_{LM}^*(\widehat{\boldsymbol{q}}_\gamma), \tag{10}$$

Eq. (6) transforms to (for each J)

$$\mathscr{T}^{L'L}_{\gamma'\gamma}(q_{\gamma'},q_\gamma)=\mathscr{V}^{L'L}_{\gamma'\gamma}(q_{\gamma'},q_\gamma)+\sum_{\gamma''=1}^{N_\alpha+N_\beta}\sum_{L''}\int\frac{dq_{\gamma''}q^2_{\gamma''}}{(2\pi)^3}\mathscr{V}^{L'L''}_{\gamma'\gamma''}(q_{\gamma'},q_{\gamma''})G_{\gamma''}\left(q^2_{\gamma''}\right)\mathscr{T}^{L''L}_{\gamma''\gamma}(q_{\gamma''},q_\gamma), \tag{11}$$

where L, L', and L'' are the angular momenta of the free particles in channels γ, γ', and γ'', respectively. The effective potentials in the representation of total angular momentum are given by

$$\mathscr{V}^{L'L}_{\gamma'\gamma}(q_{\gamma'},q_\gamma)=\sum_{m',m,M',M}\iint d\widehat{\boldsymbol{q}}_{\gamma'}d\widehat{\boldsymbol{q}}_\gamma Y^*_{L'M'}(\widehat{\boldsymbol{q}}_{\gamma'})C^{JK}_{L'M'l'm'}V_{\gamma'\gamma}(\boldsymbol{q}_{\gamma'},\boldsymbol{q}_\gamma)C^{JK}_{LMlm}Y_{LM}(\widehat{\boldsymbol{q}}_\gamma), \tag{12}$$

where C^{ab}_{cdef} are the Clebsch-Gordan coefficients of vector addition, and $Y_{LM}(\widehat{\boldsymbol{q}}_\gamma)$ are the spherical harmonics of unit vector $\widehat{\boldsymbol{q}}_\gamma$. The angular momenta of pair γ (γ') are l (l'), and M, m, K are the projections of L, l, J, respectively. Accordingly, $K=M+m=M'+m'$.

B. Effective potentials: Direct transitions

With the exception of the charge of the nucleus being changed from $Z=1$ for H to $Z=2$ for He^+, little change was required for the direct transitions when changing from a neutral (H) [4] to a charged target (He^+). The effective potentials for the $\alpha\to\alpha'$ transitions (He^+-He^+) required two main changes, the first being the subtraction of long-range Coulomb potential v_C. For He^+ this is simply $1/\rho_\alpha$. The second main change is the replacement of the spherical bessel functions j_L in the partial wave expansion of the plane wave representing the relative motion in the α channel with the regular Coulomb functions. The effective potentials for the $\beta\to\beta'$ transitions (Ps-Ps) remain effectively unchanged.

C. Effective potentials: Rearrangement

The effective potentials for the rearrangement transitions (He^{2+}-Ps) have an identical starting form to neutral atom-Ps transitions, except that the incoming plane wave of the positron is replaced by the Coulomb wave function. It is convenient to perform the replacements $\boldsymbol{\rho}_\beta\to-\boldsymbol{\rho}_\beta$ and $\boldsymbol{q}_\beta\to-\boldsymbol{q}_\beta$. Now vector $\boldsymbol{\rho}_\beta$ is the position and $\boldsymbol{q}_\beta$ is the momentum of positronium relative to the He^{2+} ion. With these changes the effective potentials for rearrangement read as

$$V_{\beta\alpha}(\boldsymbol{q}_\beta,\boldsymbol{q}_\alpha)\equiv\langle\boldsymbol{q}_\beta|\langle\psi_\beta|U_{\beta\alpha}|\psi_\alpha\rangle|\boldsymbol{q}_\alpha\rangle=\iint d\boldsymbol{\rho}_\alpha d\boldsymbol{r}_\alpha e^{-i\boldsymbol{q}_\beta\boldsymbol{\rho}_\beta}\psi^*_\beta(\boldsymbol{r}_\beta)(H_0+v-E)\psi_\alpha(\boldsymbol{r}_\alpha)\psi^{\rm C}_{\boldsymbol{q}_\alpha,\eta}(\boldsymbol{\rho}_\alpha), \tag{13}$$

where $\psi^{\rm C}_{\boldsymbol{q}_\alpha,\eta}(\boldsymbol{\rho}_\alpha)$ is the Coulomb wave function representing the motion of the electron in the field of the He^{2+} ion, $\eta=(Z-1)/q_\alpha$ in a.u., and Z is the charge of the nucleus. This will be left general for direct comparison with the e^++H system where $Z=1$. In the case of He^+, $Z=2$. How this will differ from the neutral target case will be examined in what follows.

The Hamiltonian H_0 can be taken in variables of either channel α or β

$$H_0=-\frac{1}{2}\frac{d^2}{d\boldsymbol{r}^2_\alpha}-\frac{1}{2}\frac{d^2}{d\boldsymbol{\rho}^2_\alpha}=-\frac{d^2}{d\boldsymbol{r}^2_\beta}-\frac{1}{4}\frac{d^2}{d\boldsymbol{\rho}^2_\beta}. \tag{14}$$

Split Eq. (13) into two parts according to

$$\begin{aligned}V_{\beta\alpha}(\boldsymbol{q}_\beta,\boldsymbol{q}_\alpha)=&\iint d\boldsymbol{\rho}_\alpha d\boldsymbol{r}_\alpha e^{-i\boldsymbol{q}_\beta\boldsymbol{\rho}_\beta}\psi^*_\beta(\boldsymbol{r}_\beta)[\mathscr{E}(\boldsymbol{q}_\beta,\boldsymbol{q})+v_\alpha+v_\beta]\psi_\alpha(\boldsymbol{r}_\alpha)\psi^{\rm C}_{\boldsymbol{q}_\alpha,\eta}(\boldsymbol{\rho}_\alpha)\\&+\iint d\boldsymbol{\rho}_\alpha d\boldsymbol{r}_\alpha e^{-i\boldsymbol{q}_\beta\boldsymbol{\rho}_\beta}\psi^*_\beta(\boldsymbol{r}_\beta)v_e\psi_\alpha(\boldsymbol{r}_\alpha)\psi^{\rm C}_{\boldsymbol{q}_\alpha,\eta}(\boldsymbol{\rho}_\alpha)\\=&V^{(I)}_{\beta\alpha}(\boldsymbol{q}_\beta,\boldsymbol{q}_\alpha)+V^{(II)}_{\beta\alpha}(\boldsymbol{q}_\beta,\boldsymbol{q}_\alpha),\end{aligned} \tag{15}$$

where $\mathscr{E}(\boldsymbol{q}_\beta,\boldsymbol{q})=q^2_\beta/4+{p'_\beta}^2-E\equiv q^2/2+{p'_\alpha}^2/2-E$ and

$$\boldsymbol{p}'_\beta=\boldsymbol{q}_\beta/2-\boldsymbol{q}\quad\text{and}\quad\boldsymbol{p}'_\alpha=\boldsymbol{q}_\beta-\boldsymbol{q}. \tag{16}$$

Then the two parts can be written as

$$V^{(I)}_{\beta\alpha}(\boldsymbol{q}_\beta,\boldsymbol{q}_\alpha)=\int\frac{d\boldsymbol{q}}{(2\pi)^3}\widetilde{\psi}^{\rm C}_{\boldsymbol{q},\eta}(\boldsymbol{q})[\mathscr{E}(\boldsymbol{q}_\beta,\boldsymbol{q})\widetilde{\psi}^*_\beta(\boldsymbol{p}'_\beta)\widetilde{\psi}_\alpha(\boldsymbol{p}'_\alpha)-Z\widetilde{\psi}^*_\beta(\boldsymbol{p}'_\beta)\widetilde{g}_\alpha(\boldsymbol{p}'_\alpha)-\widetilde{g}^*_\beta(\boldsymbol{p}'_\beta)\widetilde{\psi}_\alpha(\boldsymbol{p}'_\alpha)], \tag{17}$$

and

$$V^{(II)}_{\beta\alpha}(\boldsymbol{q}_\beta,\boldsymbol{q}_\alpha)=\int\frac{d\boldsymbol{q}}{(2\pi)^3}Z\widetilde{g}^{\rm C}_{\boldsymbol{q}_\alpha,\eta}(\boldsymbol{q})\widetilde{\psi}^*_\beta(\boldsymbol{p}'_\beta)\widetilde{\psi}_\alpha(\boldsymbol{p}'_\alpha), \tag{18}$$

where $\widetilde{\psi}^{\rm C}_{\boldsymbol{q},\eta}(\boldsymbol{q})$ and $\widetilde{g}^{\rm C}_{\boldsymbol{q}_\alpha,\eta}(\boldsymbol{q})$ are the Coulomb wave function and form factor in momentum space.

Transforming $V^{(I)}_{\beta\alpha}(\boldsymbol{q}_\beta,\boldsymbol{q}_\alpha)$ into the representation of total angular momentum J, then separating the radial parts of the momentum-space pseudostates and pseudo-form-factors according to $\widetilde{\psi}_\alpha(\boldsymbol{p}) = \widetilde{R}_{nl}(p)Y_{lm}(\widehat{\boldsymbol{p}})$ and $\widetilde{g}_\alpha(\boldsymbol{p}) = \widetilde{u}_{nl}(p)Y_{lm}(\widehat{\boldsymbol{p}})$ and using the following expansion for the coulomb wave function,

$$\widetilde{\psi}^{\rm C}_{\boldsymbol{q}_\alpha,\eta}(\boldsymbol{q}) = 2\pi \sum_{L''M''} Y^*_{L''M''}(\widehat{\boldsymbol{q}}_\alpha)Y_{L''M''}(\widehat{\boldsymbol{q}})\widetilde{\psi}^{\rm C}_{q_\alpha,\eta,L''}(q), \tag{19}$$

we get the following:

$$\begin{aligned}\mathscr{V}^{L'L(I)}_{\beta\alpha}(q_\beta,q_\alpha) = {}& \frac{1}{(2\pi)^2}\sum_{m',m,M',M} C^{JK}_{L'M'l'm'}C^{JK}_{LMlm}\int_0^\infty dq\, q^2\widetilde{\psi}^{\rm C}_{q_\alpha,\eta,L}(q)\int d\widehat{\boldsymbol{q}}_\beta\int d\widehat{\boldsymbol{q}}\,Y^*_{L'M'}(\widehat{\boldsymbol{q}}_\beta)Y_{LM}(\widehat{\boldsymbol{q}})Y^*_{l'm'}(\widehat{\boldsymbol{p}'}_\beta)Y_{lm}(\widehat{\boldsymbol{p}'_\alpha})\\ &\times[\mathscr{E}(\boldsymbol{q}_\beta,\boldsymbol{q})\widetilde{R}^*_{n'l'}(p'_\beta)\widetilde{R}_{nl}(p'_\alpha) - Z\widetilde{R}^*_{n'l'}(p'_\beta)\widetilde{u}_{nl}(p'_\alpha) - \widetilde{u}^*_{n'l'}(p'_\beta)\widetilde{R}_{nl}(p'_\alpha)].\end{aligned} \tag{20}$$

Decomposing the spherical harmonics of the direction of the relative motion in pairs α and β one gets

$$\begin{aligned}\mathscr{V}^{L'L(I)}_{\beta\alpha}(q_\beta,q_\alpha) = {}& \frac{1}{\pi}\sum_{m',m,M',M} C^{JK}_{L'M'l'm'}C^{JK}_{LMlm}\int_0^\infty dq\, q^2\widetilde{\psi}^{\rm C}_{q_\alpha,\eta,L}(q)\sum_{l'_1,m'_1,m'_2} C^{l'm'}_{l'_1m'_1l'_2m'_2}\frac{[l'!]}{[l'_1!l'_2!]}q^{l'_1}_\beta(-q)^{l'_2}2^{-l'_1}\sum_{l_1,m_1,m_2}C^{lm}_{l_1m_1l_2m_2}\\ &\times\frac{[l!]}{[l_1!l_2!]}q^{l_1}_\beta(-q)^{l_2}\iint d\widehat{\boldsymbol{q}}_\beta\, d\widehat{\boldsymbol{q}}\,F^{(I)}(\boldsymbol{q}_\beta,\boldsymbol{q})Y^*_{L'M'}(\widehat{\boldsymbol{q}}_\beta)Y_{LM}(\widehat{\boldsymbol{q}})Y_{l_1m_1}(\widehat{\boldsymbol{q}}_\beta)Y^*_{l'_1m'_1}(\widehat{\boldsymbol{q}}_\beta)Y_{l_2m_2}(\widehat{\boldsymbol{q}})Y^*_{l'_2m'_2}(\widehat{\boldsymbol{q}}).\end{aligned} \tag{21}$$

Here

$$F^I(\boldsymbol{q}_\beta,\boldsymbol{q}) = \mathscr{E}(\boldsymbol{q}_\beta,\boldsymbol{q})\frac{\widetilde{R}^*_{n'l'}(p'_\beta)\widetilde{R}_{nl}(p'_\alpha)}{{p'_\alpha}^{l'}{p'_\alpha}^{l}} - Z\frac{\widetilde{R}^*_{n'l'}(p'_\beta)\widetilde{u}_{nl}(p'_\alpha)}{{p'_\beta}^{l'}{p'_\alpha}^{l}} - \frac{\widetilde{u}^*_{n'l'}(p'_\beta)\widetilde{R}_{nl}(p'_\alpha)}{{p'_\beta}^{l'}{p'_\alpha}^{l}}, \tag{22}$$

and $[l] = \sqrt{[2l+1]}$, $[l!] = \sqrt{[2l+1]!}$. Combining two spherical harmonics of the same relative motion in channels α and β and some rearrangement we get

$$\begin{aligned}\mathscr{V}^{L'L(I)}_{\beta\alpha}(q_\beta,q_\alpha) = {}& \frac{1}{(2\pi)^2}\sum_{m',m,M',M} C^{JK}_{L'M'l'm'}C^{JK}_{LMlm}\sum_{l'_1,m'_1,m'_2} C^{l'm'}_{l'_1m'_1l'_2m'_2}\frac{[l'!]}{[l'_1!l'_2!]}q^{l'_1}_\beta(-1)^{l'_2}2^{-l'_1}\sum_{l_1,m_1,m_2}C^{lm}_{l_1m_1l_2m_2}\\ &\times\frac{[l!]}{[l_1!l_2!]}q^{l_1}_\beta(-1)^{l_2}\sum_{l''_1m''_1}\frac{[l_1][l'_1]}{[l''_1]}C^{l''_1m''_1}_{l_1m_1l'_1m'_1}C^{l''_10}_{l_10l'_10}(-1)^{m_1}\sum_{l''_2m''_2}\frac{[l_2][l'_2]}{[l''_2]}C^{l''_2m''_2}_{l_2m_2l'_2m'_2}C^{l''_20}_{l_20l'_20}(-1)^{m'_2}\\ &\times\int_0^\infty dq\, q^{l_2+l'_2+2}\widetilde{\psi}^{\rm C}_{q_\alpha,\eta,L}(q)\iint d\widehat{\boldsymbol{q}}_\beta\, d\widehat{\boldsymbol{q}}\,F^{(I)}(\boldsymbol{q}_\beta,\boldsymbol{q})Y^*_{L'M'}(\widehat{\boldsymbol{q}}_\beta)Y_{LM}(\widehat{\boldsymbol{q}})Y^*_{l''_1m''_1}(\widehat{\boldsymbol{q}}_\beta)Y_{l''_2m''_2}(\widehat{\boldsymbol{q}}).\end{aligned} \tag{23}$$

Now we expand $F^{(I)}(\boldsymbol{q}_\beta,\boldsymbol{q})$ as

$$F^{(I)}(\boldsymbol{q}_\beta,\boldsymbol{q}) = 2\pi\sum_{\lambda,\mu}\mathscr{F}^{(I)}_\lambda(q_\beta,q)Y^*_{\lambda\mu}(\widehat{\boldsymbol{q}}_\beta)Y_{\lambda\mu}(\widehat{\boldsymbol{q}}), \tag{24}$$

where the expansion coefficients are given by

$$\mathscr{F}^{(I)}_\lambda(q_\beta,q) = \int_{-1}^1 dz\, F^{(I)}(\boldsymbol{q}_\beta,\boldsymbol{q})P_\lambda(z), \tag{25}$$

and $z = \widehat{\boldsymbol{q}}_\beta\cdot\widehat{\boldsymbol{q}}$. Then integrating over the angular momenta we get

$$\begin{aligned}\mathscr{V}^{L'L(I)}_{\beta\alpha}(q_\beta,q_\alpha) = {}& \frac{1}{8\pi^2}\sum_{m',m,M',M} C^{JK}_{L'M'l'm'}C^{JK}_{LMlm}\sum_{l'_1,m'_1,m'_2} C^{l'm'}_{l'_1m'_1l'_2m'_2}\frac{[l'!]}{[l'_1!l'_2!]}q^{l'_1}_\beta(-1)^{l'_2}2^{-l'_1}\sum_{l_1,m_1,m_2}C^{lm}_{l_1m_1l_2m_2}\frac{[l!]}{[l_1!l_2!]}q^{l_1}_\beta(-1)^{l_2}\\ &\times\sum_{l''_1m''_1}\frac{[l_1][l'_1]}{[l''_1]}C^{l''_1m''_1}_{l_1m_1l'_1m'_1}C^{l''_10}_{l_10l'_10}(-1)^{m_1+m''_1}\sum_{l''_2m''_2}\frac{[l_2][l'_2]}{[l''_2]}C^{l''_2m''_2}_{l_2m_2l'_2m'_2}C^{l''_20}_{l_20l'_20}(-1)^{m'_2+m''_2}\sum_{\lambda,\mu}\frac{[L'][\lambda]}{[l''_1]}C^{l''_1m''_1}_{L'M'\lambda\mu}\\ &\times C^{l''_10}_{L'0\lambda0}\frac{[L][\lambda]}{[l''_2]}C^{l''_2m''_2}_{LM\lambda\mu}C^{l''_20}_{L0\lambda0}\int_0^\infty dq\, q^{l_2+l'_2+2}\widetilde{\psi}^{\rm C}_{q_\alpha,\eta,L}(q)\mathscr{F}^{(I)}_\lambda(q_\beta,q)\\ = {}&\sum_{l'_1}\frac{[l'!]}{[l'_1!l'_2!]}q^{l'_1}_\beta 2^{-l'_1-1}\sum_{l_1}\frac{[l!]}{[l_1!l_2!]}q^{l_1}_\beta\sum_{l''_1}\frac{[l_1][l'_1]}{[l''_1]}C^{l''_10}_{l_10l'_10}\sum_{l''_2}\frac{[l_2][l'_2]}{[l''_2]}C^{l''_20}_{l_20l'_20}\sum_\lambda\frac{[L'][\lambda]}{[l''_1]}C^{l''_10}_{L'0\lambda0}\frac{[L][\lambda]}{[l''_2]}C^{l''_20}_{L0\lambda0}\\ &\times I^{\lambda(I)}_{\beta,\alpha}(q_\beta,q_\alpha)\sum_{m',m,M',M,m'_1,m'_2,m_1,m_2m''_1m''_2,\mu}(-1)^{m_1+m''_1+m'_2+m''_2+l'_2+l_2}C^{JK}_{L'M'l'm'}C^{JK}_{LMlm}C^{l'm'}_{l'_1m'_1l'_2m'_2}C^{lm}_{l_1m_1l_2m_2}\\ &\times C^{l''_1m''_1}_{l_1m_1l'_1m'_1}C^{l''_2m''_2}_{l_2m_2l'_2m'_2}C^{l''_1m''_1}_{L'M'\lambda\mu}C^{l''_2m''_2}_{LM\lambda\mu},\end{aligned} \tag{26}$$

where

$$I^{\lambda(I)}_{\beta,\alpha}(q_\beta,q_\alpha) = \frac{1}{(2\pi)^2}\int_0^\infty dq\, q^{l_2+l_2'+2}\widetilde{\psi}^{\mathrm{C}}_{q_\alpha,\eta,L}(q)\mathscr{F}^{(I)}_\lambda(q_\beta,q). \tag{27}$$

Summing over all projections of the angular momenta leads to

$$\mathscr{V}^{L'L(I)}_{\beta\alpha}(q_\beta,q_\alpha) = \frac{1}{4\pi^2}[l'lL'Ll'!l!](-1)^{J+L'}\sum_{l_1'}\frac{[l_1'l_2']}{[l_1'!l_2'!]}2^{-l_1'-1}\frac{[l_1l_2]}{[l_1!l_2!]}q_\beta^{l_1+l_1'}\sum_{l_1''}C^{l_1''0}_{l_10l_1'0}\sum_{l_2''}C^{l_2''0}_{l_20l_2'0}\sum_\lambda[\lambda]^2C^{l_1''0}_{L'0\lambda0}C^{l_2''0}_{L0\lambda0}$$
$$\times\begin{Bmatrix} l_1 & l & J & l' \\ l_2 & L & L' & l_1' \\ l_2' & l_2'' & \lambda & l_1'' \end{Bmatrix} I^{\lambda(I)}_{\beta,\alpha}(q_\beta,q_\alpha). \tag{28}$$

Next we transform $V^{(II)}_{\beta\alpha}(\boldsymbol{q}_\beta,\boldsymbol{q}_\alpha)$:

$$\mathscr{V}^{L'L(II)}_{\beta\alpha}(q_\beta,q_\alpha) = \frac{1}{(2\pi)^3}\sum_{m',m,M',M} C^{JK}_{L'M'l'm'}C^{JK}_{LMlm}\iint d\widehat{\boldsymbol{q}}_\beta\, d\widehat{\boldsymbol{q}}_\alpha Y^*_{L'M'}(\widehat{\boldsymbol{q}}_\beta)Y_{LM}(\widehat{\boldsymbol{q}}_\alpha)\int dq\, Z\widetilde{g}^{\mathrm{C}}_{\boldsymbol{q}_\alpha,\eta}(q)\widetilde{\psi}^*_\beta(\boldsymbol{p}'_\beta)\widetilde{\psi}_\alpha(\boldsymbol{p}'_\alpha). \tag{29}$$

Again, separating out the radial components of the momentum-space pseudostates and pseudoform factors and expanding the momentum-space Coulomb form factor according to

$$\widetilde{g}^{\mathrm{C}}_{\boldsymbol{q}_\alpha,\eta}(\boldsymbol{q}) = 2\pi\sum_{L''M''}Y^*_{L''M''}(\widehat{\boldsymbol{q}}_\alpha)Y_{L''M''}(\widehat{\boldsymbol{q}})\widetilde{u}^{\mathrm{C}}_{q_\alpha,\eta,L''}(q), \tag{30}$$

we get the following:

$$\mathscr{V}^{L'L(II)}_{\beta\alpha}(q_\beta,q_\alpha) = \frac{1}{(2\pi)^2}\sum_{m',m,M',M} C^{JK}_{L'M'l'm'}C^{JK}_{LMlm}\int d\widehat{\boldsymbol{q}}_\beta\int d\widehat{\boldsymbol{q}}\, Y^*_{L'M'}(\widehat{\boldsymbol{q}}_\beta)Y_{LM}(\widehat{\boldsymbol{q}})Y^*_{l'm'}(\widehat{\boldsymbol{p}'}_\beta)Y_{lm}(\widehat{\boldsymbol{p}'_\alpha})$$
$$\times\int_0^\infty dq\, q^2\widetilde{u}^{\mathrm{C}}_{q_\alpha,\eta,L}(q)Z\widetilde{R}^*_{n'l'}(p'_\beta)\widetilde{R}_{nl}(p'_\alpha), \tag{31}$$

which has the same form as Eq. (20), the only differences being that the partial wave Coulomb wave function $\widetilde{\psi}^{\mathrm{C}}_{q_\alpha,\eta,L}(q)$ is replaced by the form factor $\widetilde{u}^{\mathrm{C}}_{q_\alpha,\eta,L}(q)$, and $F^{(II)}$ is given as

$$F^{II}(\boldsymbol{q}_\beta,\boldsymbol{q}) = Z\frac{\widetilde{R}^*_{n'l'}(p'_\beta)\widetilde{R}_{nl}(p'_\alpha)}{p'^{l'}_\alpha p'^{l}_\alpha}. \tag{32}$$

Combining all results together for rearrangement we have

$$\mathscr{V}^{L'L(I)}_{\beta\alpha}(q_\beta,q_\alpha) = [l'lL'Ll'!l!](-1)^{J+L'}\sum_{l_1'}\frac{[l_1'l_2']}{[l_1'!l_2'!]}2^{-l_1'-1}\sum_{l_1}\frac{[l_1l_2]}{[l_1!l_2!]}q_\beta^{l_1+l_1'}\sum_{l_1''}C^{l_1''0}_{l_10l_1'0}\sum_{l_2''}C^{l_2''0}_{l_20l_2'0}\sum_\lambda[\lambda]^2C^{l_1''0}_{L'0\lambda0}C^{l_2''0}_{L0\lambda0}$$
$$\times\begin{Bmatrix} l_1 & l & J & l' \\ l_2 & L & L' & l_1' \\ l_2' & l_2'' & \lambda & l_1'' \end{Bmatrix} I^{\lambda}_{\beta\alpha}(q_\beta,q_\alpha), \tag{33}$$

where

$$I^{\lambda}_{\beta,\alpha}(q_\beta,q_\alpha) = \frac{1}{(2\pi)^2}\int_0^\infty dq\, q^{l_2'+l_2+2}\left[\widetilde{\psi}^{\mathrm{C}}_{q_\alpha,\eta,L}(q)\mathscr{F}^{I}_\lambda(q_\beta,q) + \widetilde{u}^{\mathrm{C}}_{q_\alpha,\eta,L}(q)\mathscr{F}^{II}_\lambda(q_\beta,q)\right]. \tag{34}$$

According to Eremenko *et al.* [32] the Coulomb wave function and its partial wave expansion is given by

$$\widetilde{\psi}^{\mathrm{C}}_{q_\alpha,\eta,L}(q) = \int_{-1}^{+1}dz\, P_L(z)\widetilde{\psi}^{\mathrm{C}}_{\boldsymbol{q},\eta}(\boldsymbol{q}) = -\frac{4\pi e^{\pi\eta/2}}{qq_\alpha}\lim_{\gamma\to+0}\frac{d}{d\gamma}\left[\left(\frac{q^2-(q_\alpha+i\gamma)^2}{2qq_\alpha}\right)^{i\eta}(\zeta^2-1)^{-i\eta/2}Q^{i\eta}_L(\zeta)\right], \tag{35}$$

where $\zeta = (q^2+q_\alpha^2+\gamma^2)/2qq_\alpha$. The Coulomb form factor has a similar form; however, in this case there is no need for $-d/d\gamma$.

If we set $Z=1$, and hence $\eta=0$, the Coulomb wave function becomes

$$\widetilde{\psi}^{\mathrm{C}}_{q_\alpha,0,L}(q) = -4^2\pi\frac{\pi\delta(q\pm q_\alpha)}{(q\mp q_\alpha)^2}(L+1)\left[Q_{L+1}\left(\frac{q^2+q_\alpha^2}{2qq_\alpha}\right)-\left(\frac{q^2+q_\alpha^2}{2qq_\alpha}\right)Q_L\left(\frac{q^2+q_\alpha^2}{2qq_\alpha}\right)\right]. \tag{36}$$

The form factor becomes

$$\widetilde{u}^{\mathrm{C}}_{q_\alpha,0,L}(q) = \frac{4\pi}{qq_\alpha} Q_L\left(\frac{q^2+q_\alpha^2}{2qq_\alpha}\right). \tag{37}$$

Substituting this back into Eq. (34) gives

$$\begin{aligned} I^{\lambda}_{\beta,\alpha}(q_\beta,q_\alpha) &= \frac{-1}{\pi}\int_0^\infty dq\, q^{l_2'+l_2+2}\frac{4\pi\delta(q\pm q_\alpha)}{(q\mp q_\alpha)^2}(L+1)\left[Q_{L+1}\left(\frac{q^2+q_\alpha^2}{2qq_\alpha}\right)-\left(\frac{q^2+q_\alpha^2}{2qq_\alpha}\right)Q_L\left(\frac{q^2+q_\alpha^2}{2qq_\alpha}\right)\right]\mathscr{F}^{I}_{\lambda}(q_\beta,q) \\ &\quad - \frac{q^{l_2'+l_2+2}}{qq_\alpha}Q_L\left(\frac{q^2+q_\alpha^2}{2qq_\alpha}\right)\mathscr{F}^{II}_{\lambda}(q_\beta,q) \\ &= q_\alpha^{l_2'+l_2}\mathscr{F}^{I}_{\lambda}(q_\beta,q_\alpha) + \frac{1}{\pi q_\alpha}\int_0^\infty dq\, q^{l_2'+l_2+1}Q_L\left(\frac{q^2+q_\alpha^2}{2qq_\alpha}\right)\mathscr{F}^{II}_{\lambda}(q_\beta,q). \end{aligned} \tag{38}$$

Since $\lim_{x\to 1} Q_{L+1}(x) - xQ_L(x) = -1/(L+1)$, this reduces to the result obtained for neutral targets [4].

III. DETAILS OF CALCULATIONS

The effective potentials for the direct matrix elements require integration over two regular one-dimensional integrals. This is performed using a fine radial mesh and can be calculated much quicker than the rearrangement matrix elements.

As shown in the preceding section, the positronium-formation matrix elements have the same coupling of 12 angular momenta as seen in e^++H scattering, leading to finite angular momentum sums and two-dimensional integrals. Compact analytical expressions for the momentum-space pseudostates and corresponding form factors derived in Ref. [4] are used in this approach as well. The main difference was the inclusion of the momentum-space Coulomb wave function and its corresponding form factor. Both have compact analytical forms. For the wave function we make use of the FORTRAN code developed by Eremenko *et al.* [32]. However, the code was slightly altered to suit our needs, the most notable change being the removal of the complex phase factor. As was the case in the previous Ps-formation calculations, this integral has a singularity at $q = q_\alpha$. However, unlike the logarithmic singularity from Q_L, this singularity is complex and arises from $\widetilde{\psi}^{\mathrm{C}}_{q_\alpha,\eta,L}$ and $\widetilde{u}^{\mathrm{C}}_{q_\alpha,\eta,L}$. Instead of having two separate integrals for the Coulomb wave function and form factor, it is preferable to relate the two together under one function as

$$\widetilde{\psi}^{\mathrm{C}}_{q_\alpha,\eta,L}(q) = -\frac{4\pi e^{\pi\eta/2}}{qq_\alpha}\lim_{\gamma\to+0}\frac{d}{d\gamma}\left[\left(\frac{q^2-(q_\alpha+i\gamma)^2}{2qq_\alpha}\right)^{i\eta}(\zeta^2-1)^{-i\eta/2}Q_L^{i\eta}(\zeta)\right], \tag{39}$$

$$\widetilde{u}^{\mathrm{C}}_{q_\alpha,\eta,L}(q) = \frac{4\pi e^{\pi\eta/2}}{qq_\alpha}\lim_{\gamma\to+0}\left[\left(\frac{q^2-(q_\alpha+i\gamma)^2}{2qq_\alpha}\right)^{i\eta}(\zeta^2-1)^{-i\eta/2}Q_L^{i\eta}(\zeta)\right]. \tag{40}$$

We can expand the derivative as follows

$$\begin{aligned} &\frac{d}{d\gamma}\left[\left(\frac{q^2-(q_\alpha+i\gamma)^2}{2qq_\alpha}\right)^{i\eta}(\zeta^2-1)^{-i\eta/2}Q_L^{i\eta}(\zeta)\right] \\ &= \left(\frac{q^2-(q_\alpha+i\gamma)^2}{2qq_\alpha}\right)^{i\eta}(\zeta^2-1)^{-i\eta/2}\left[\frac{2\eta q_\alpha}{q^2-(q_\alpha+i\gamma)^2}Q_L^{i\eta}(\zeta)+\gamma\left(\frac{i2\eta Q_L^{i\eta}(\zeta)}{q^2-(q_\alpha+i\gamma)^2}+\frac{Q_L^{i\eta+1}(\zeta)}{qq_\alpha(\zeta^2-1)^{1/2}}\right)\right]. \end{aligned} \tag{41}$$

The first term and the remaining terms have broadly similar behaviors, so when the limit $\gamma \to 0$ is taken, only the first term survives. Therefore, we get

$$\widetilde{\psi}^{\mathrm{C}}_{q_\alpha,\eta,L}(q) = -\frac{4\pi e^{\pi\eta/2}}{qq_\alpha}\frac{2\eta q_\alpha}{q^2-q_\alpha^2}\left[\frac{(q_\alpha+i0)^2-q^2}{2qq_\alpha}\right]^{i\eta}(\zeta^2-1)^{-i\eta/2}Q_L^{i\eta}(\zeta) \tag{42}$$

$$\widetilde{u}^{\mathrm{C}}_{q_\alpha,\eta,L}(q) = \frac{4\pi e^{\pi\eta/2}}{qq_\alpha}\left[\frac{q^2-(q_\alpha+i0)^2}{2qq_\alpha}\right]^{i\eta}(\zeta^2-1)^{-i\eta/2}Q_L^{i\eta}(\zeta) = \frac{q_\alpha^2-q^2}{2\eta q_\alpha}\widetilde{\psi}^{\mathrm{C}}_{q_\alpha,\eta,L}(q). \tag{43}$$

Accordingly Eq. (34) reduces to

$$I^{\lambda}_{\beta,\alpha}(q_\beta,q_\alpha) = \frac{1}{(2\pi)^2}\int_0^\infty dq\, q^{l_2'+l_2+2}\widetilde{\psi}^{\mathrm{C}}_{q_\alpha,\eta,L}(q)\left[\mathscr{F}^{I}_{\lambda}(q_\beta,q)+\frac{q_\alpha^2-q^2}{2\eta q_\alpha}\mathscr{F}^{II}_{\lambda}(q_\beta,q)\right], \tag{44}$$

leaving the function in a more compact form with the singularity in one part and the regular functions in the other. For handling the singularities we use a subtraction method similar to the one used by Mitroy [33]. Near the singularity the momentum-space Coulomb wave functions have the following form:

$$\widetilde{\psi}^{\mathrm{C}}_{q_\alpha,\eta,L}(q) = -\frac{8\pi e^{-\pi\eta/2}}{q}\left(\frac{(q+q_\alpha)^2}{4qq_\alpha}\right)^{L}\mathrm{Im}(\mathscr{D}), \tag{45}$$

where

$$\mathscr{D} = \Gamma(1+i\eta)e^{-i\sigma_L}\frac{(q+q_\alpha)^{i\eta-1}}{(q-q_\alpha)^{i\eta+1}}\,{}_2F_1\left(-L,-i\eta-L,1-i\eta,\frac{(q-q_\alpha)^2}{(q+q_\alpha)^2}\right). \tag{46}$$

The singular behavior is contained within the term

$$\frac{(q+q_\alpha)^{i\eta-1}}{(q-q_\alpha)^{i\eta+1}}, \tag{47}$$

with the complex exponents introducing oscillations. Since as $q \to q_\alpha$ the hypergeometric and the $[(q+q_\alpha)^2/4qq_\alpha]^L$ terms tend to 1, ignoring these terms would make for a good subtracting function, e.g.,

$$\widetilde{\psi}^{\rm Sub}_{q_\alpha,\eta,L}(q) = -\frac{8\pi e^{-\pi\eta/2}}{q}{\rm Im}\left[\Gamma(1+i\eta)e^{-i\sigma_L}\frac{(q+q_\alpha)^{i\eta-1}}{(q-q_\alpha)^{i\eta+1}}\right]. \tag{48}$$

Using this in Eq. (44) within some range from q_1 to q_2, where q_1 and q_2 are points just below and above the singularity q_α, we have

$$\begin{aligned} I^\lambda_{\beta,\alpha}(q_\beta,q_\alpha) =& \frac{1}{(2\pi)^2}\int_{q_1}^{q_2} dq\left[q^{l'_2+l_2+2}\widetilde{\psi}^{\rm C}_{q_\alpha,\eta,L}(q)\left(\mathscr{F}^I_\lambda(q_\beta,q)+\frac{q_\alpha^2-q^2}{2\eta q_\alpha}\mathscr{F}^{II}_\lambda(q_\beta,q)\right)\right. \\ &\left. - q_\alpha^{l'_2+l_2+1}q\widetilde{\psi}^{\rm Sub}_{q_\alpha,\eta,L}(q)\mathscr{F}^I_\lambda(q_\beta,q_\alpha)\right] + \mathscr{F}^I_\lambda(q_\beta,q_\alpha)\frac{q_\alpha^{l'_2+l_2+1}}{(2\pi)^2}\int_{q_1}^{q_2} dq\, q\widetilde{\psi}^{\rm Sub}_{q_\alpha,\eta,L}(q), \end{aligned} \tag{49}$$

where we can make use of

$$\int dq\, q\widetilde{\psi}^{\rm Sub}_{q_\alpha,\eta,L}(q) = -8\pi e^{-\pi\eta/2}{\rm Im}\left[\Gamma(1+i\eta)e^{-i\sigma_L}\int dq\frac{(q+q_\alpha)^{i\eta-1}}{(q-q_\alpha)^{i\eta+1}}\right] = -8\pi e^{-\pi\eta/2}{\rm Re}\left[\Gamma(1+i\eta)e^{-i\sigma_L}\frac{1}{2\eta q_\alpha}\left(\frac{q+q_\alpha}{q-q_\alpha}\right)^{i\eta}\right]. \tag{50}$$

Due to the oscillatory nature of this function and how its phase depends on η, as the momentum of the incoming positron q_α decreases and η increases, the integrand becomes more oscillatory and harder to manage. It is also possible to further increase the accuracy of the subtraction for lower q_α values by including the second term of the Taylor expansion for $\mathscr{F}^I_\lambda(q_\beta,q)$:

$$f_l(q) \approx f_l(q_\alpha) + \frac{df_l(q)}{dq}\Delta q \approx f_l(q_\alpha) + \frac{f_l(q_2)-f_l(q_1)}{q_2-q_1}(q-q_\alpha), \tag{51}$$

and making use of

$$\begin{aligned} \int dq\, q(q-q_\alpha)\widetilde{\psi}^{\rm Sub}_{q_\alpha,\eta,L}(q) =& -8\pi e^{-\pi\eta/2}{\rm Im}\left[\Gamma(1+i\eta)e^{-i\sigma_L}\int dq\frac{(q+q_\alpha)^{i\eta-1}}{(q-q_\alpha)^{i\eta}}\right] \\ =& -8\pi e^{-\pi\eta/2}{\rm Im}\left[\Gamma(1+i\eta)e^{-i\sigma_L}\frac{1}{1-i\eta}\left(\frac{q+q_\alpha}{q-q_\alpha}\right)^{i\eta-1}{}_2F_1\left(1,1-i\eta,2-i\eta,\frac{q-q_\alpha}{q+q_\alpha}\right)\right]. \end{aligned} \tag{52}$$

However, even this extension starts to break down for even lower values of q_α and further expansions have the potential to introduce more numerical errors. Fortunately, for $\eta > 0$ as $\eta \to \infty$ the Coulomb wave function tends to zero at an exponential rate, so the contribution from these calculations becomes negligible and can therefore be ignored. Conversely, for $\eta < 0$, the subtraction method can generate more accurate results for higher $|\eta|$ values, but these do not tend to zero like before. So for positron scattering on a positive ion the method above is viable for integrating over the singularity; for negative ions more work will be required for smaller q_α values, but that is for future development.

In order for these terms to be be solved using real arithmetic the complex phase factor $e^{i\sigma_L} = {\rm Arg}[\Gamma(L+1+i\eta)]$ arising from the Coulomb functions has been removed. This step is repeated in direct transitions as well as rearrangement. This factor is reinstated once the system of coupled equations is solved.

The transition matrix elements are calculated by solving a system of coupled momentum-space integral equations (6). These are solved using real arithmetic by following the standard technique of converting the complex T matrix to a real K matrix as typically done in the CCC method [3]. From here the numerical solutions of these equations are calculated using standard quadrature rules. The complex terms $e^{i\sigma_L}$ arising from the Coulomb wave functions can be trivially factored out as described in Ref. [2].

IV. RESULTS

A. Convergence study

The foundation of the CCC method is that as the size of the basis N is systematically increased the results should converge to the solution of the underlying Schrödinger equation. However, since the two-center case is ill-conditioned, increasing the basis size on both centers requires some care.

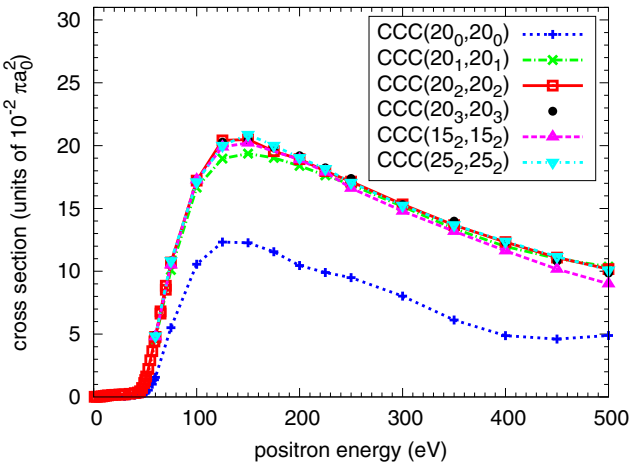

FIG. 2. Total cross sections for e^+-He^+ scattering.

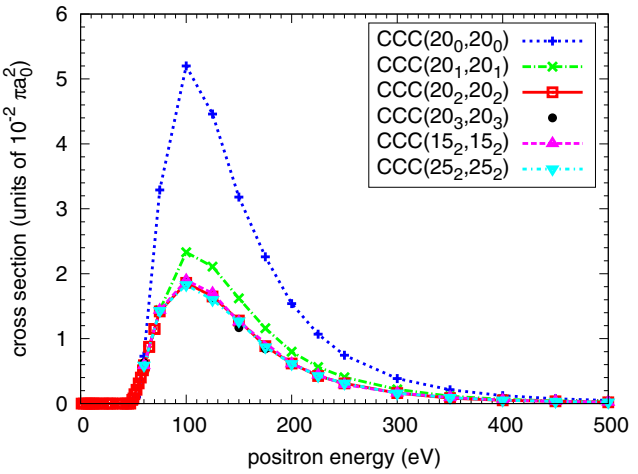

FIG. 4. Total Ps-formation cross sections for e^+-He^+ scattering.

For convergence studies, calculations are performed with basis sizes $N = \sum_{l=0}^{l_{\max}} N_l$ by increasing the size of N_l for each angular momentum l and maximum angular momentum $l_{\max}$ on both centers. To limit the number of free parameters, typically the same number of Laguerre-based states are used on both centers. Furthermore, we set $N_l = N_0 - l$ requiring that only N_0 and $l_{\max}$ need to be varied in convergence studies. The corresponding calculations are denoted as CCC($N_{0l_{\max}}^{\mathrm{T}}$, $N_{0l_{\max}}^{\mathrm{Ps}}$) in the figures. For all the bases, the fall-off parameter λ_l is set to 2.0 for He^+ and 0.5 for Ps independent of l.

In what follows we do not incorporate the ionic target Rutherford scattering term in the elastic cross section. This ensures that the elastic, and hence total, cross sections remain finite allowing for convergence checking for each partial wave of total orbital angular momentum. Rather than providing results for each partial wave J, instead we present the results converged with respect to the partial wave sum. Presently, Eq. (11) was solved explicitly for $0 \leqslant J \leqslant 20$.

The convergence studies for the total, total breakup, and total Ps-formation cross sections are shown in Figs. 2–4, respectively. In each case there are sets of calculations with $N_0 = 20$ for $l_{\max} = 0,1,2,3$ to test convergence in the orbital angular momentum of the included states. The inclusion of the p states in addition to the s states has made a significant difference to the results. Further inclusion of the d states was less substantial, but contributed an additional 20% at the maximum for the breakup cross section. Inclusion of the f states appeared to have practically no effect, which is very similar to calculations for e^+ scattering on H [4] and He [19]. Additional calculations were performed with $l_{\max} = 2$ and $N_0 = 15$ and 25 to check convergence with N_0. For the total cross section the main noticeable difference for the various N_0 calculations is that the $N_0 = 15$ calculations seem to underestimate the larger calculations for energies greater than 400 eV. This could be due to the number of positive-energy pseudostates being insufficient at these energies. For the total breakup cross section there is some variation for the larger cross section values but this is typically within 1%. For the total Ps-formation cross section there in no noticeable difference between these three sets of calculations.

It can be observed that the basis CCC(20$_2$,20$_2$) is large enough to generate accurate e^+-He^+ scattering cross sections at all energies considered.

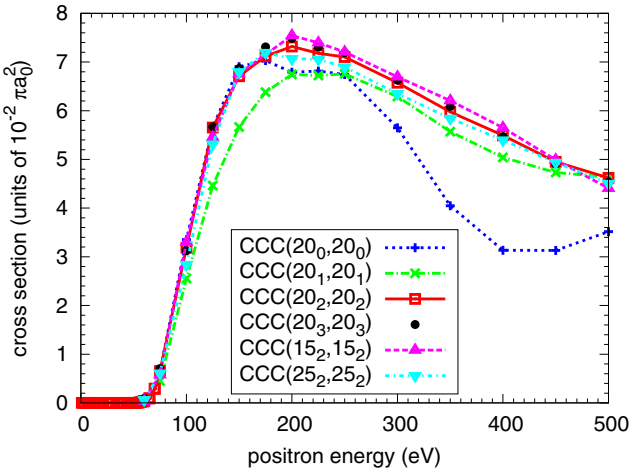

FIG. 3. Total breakup cross sections for e^+-He^+ scattering.

B. Internal consistency

The results of the internal consistency checks are given in Figs. 5 and 6 for the total and electron-loss cross sections, respectively. In both cases the two-center CCC(20$_2$,20$_2$) are compared with single-center CCC(30$_9$,0). The inserts highlight the region from 40 to 60 eV to further examine the differences around the breakup threshold of 54.4 eV. For the total cross section, there appears to be very little difference between the two expansions. The same can be said for the electron-loss cross section at first glance. However, when the corresponding insert is examined, it can be seen that the threshold for electron loss is around 55 eV for the single-center results and around 48 eV for the two-center ones. This is to be expected since the ionization and Ps($1s$) formation thresholds are 54.4 and 47.6 eV, respectively, and since the single-center expansion has no possibility for Ps formation, the only way for it to lose an electron is via ionization. This is further validated by the fact that the electron-loss (Ps-formation plus breakup) cross

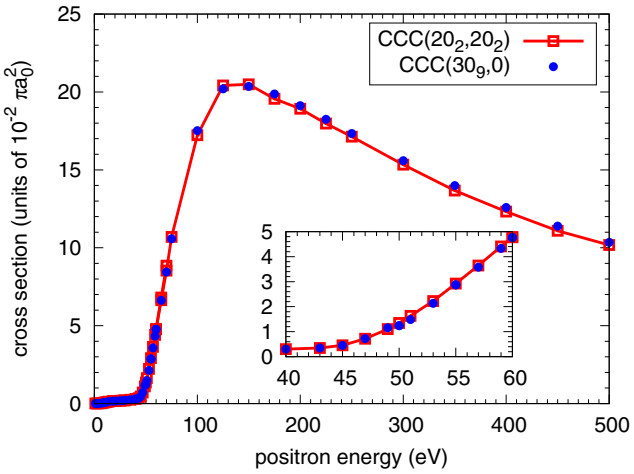

FIG. 5. Total cross sections for e^+-He^+ scattering. The insert highlights the region around the ionization threshold.

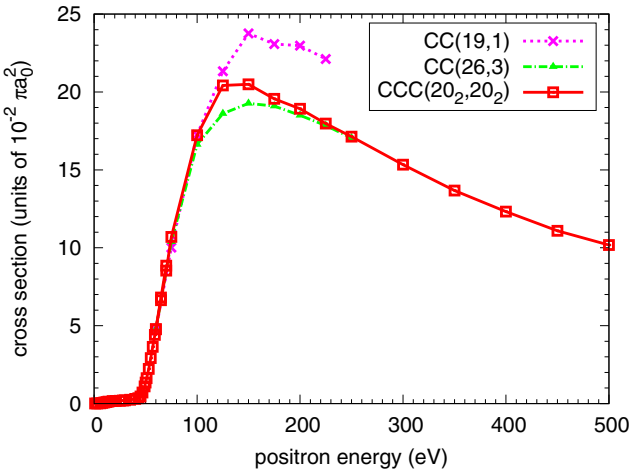

FIG. 7. Total cross sections for e^+-He^+ scattering. Close-coupling results are from Bransden *et al.* [8].

section for the two-center expansion in this region is entirely due to Ps formation.

These two checks also show that the inclusion of the new Ps-formation matrix elements conserves the unitarity of the close-coupling formalism. This is clear for a single-center calculation which utilizes a complete basis, but less clear when a two-center expansion is utilized using two independently complete bases. The agreement between the two calculations indicates no double counting problems. Since cross sections are defined at infinite separations of the reacting particles the two-center expansions do not overlap at infinity due to being square-integrable. Hence convergence to the same result is demonstrably achieved in one- and two-center calculations, but the latter is much more ill conditioned (requires higher internal numerical precision).

C. Comparison with other theories

Unlike positron scattering on hydrogen, the problem of positron scattering on He^+ has not been studied much in depth. Currently no experimental results exist for this system and

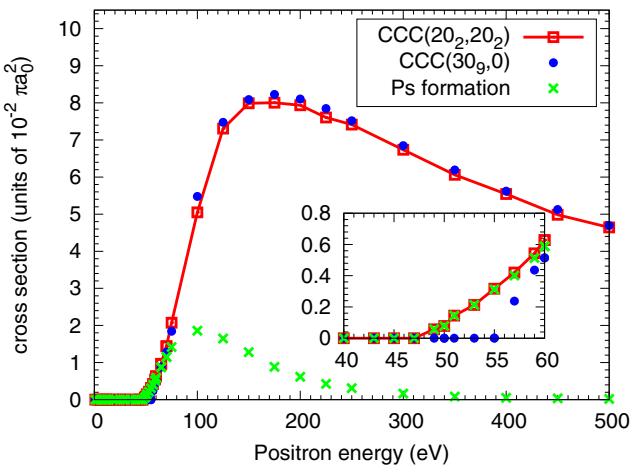

FIG. 6. Electron-loss cross sections for e^+-He^+ scattering. The insert highlights the region around the ionization threshold.

most other theoretical calculations focus on elastic scattering close to the threshold. Bransden *et al.* [8] has produced results above the ionization threshold for various processes using a close-coupling approach. Using the EFS-CDW method, Zhang *et al.* [10] have also produced results in this region but only for the Ps-formation cross sections.

Figure 7 shows the total cross sections from CCC calculations compared to the CC calculations from Bransden *et al.* [8]. Excellent agreement is found between the CCC results and both CC(19,1) and CC(26,3) results up to 100 eV. Above that the CC(19,1) results begin to overestimate the CCC results. The CC(26,3) results underestimate the CCC results until around 200 eV where the agreement is again very good.

Figures 8(a)–8(c) show the total breakup, Ps-formation, and (their sum) electron-loss cross sections, respectively. There is some disagreement between the present CCC results and the CC results of Bransden *et al.* [8] for the breakup cross section. The two CC results are visibly lower than the CCC results. Given the good agreement for Ps formation, which is dominated by Ps in the ground state, the discrepancy for the breakup cross section is likely to be due to insufficiently many positive-energy target states in the CC calculations. The EFS-CDW results of Zhang *et al.* [10], available only for Ps formation, are considerably higher than the CC and CCC results. In these calculations Ps($n = 1$–4) were used to approximate the total Ps-formation cross sections, so it is possible that the cross sections for Ps($n > 2$) are higher than expected; however, these were not presented by Zhang *et al.* [10].

Figure 9 shows the elastic-scattering, $2s$ and $2p$ excitation cross sections. For all three processes the three sets of calculations generate consistent results up until around 100 eV when they start to diverge. For elastic scattering the CC calculations approach the CCC calculations as the basis size increases. The process with the smallest cross section, $2s$ excitation, overall shows excellent agreement between CC(26,3) and CCC results. The process with the largest cross section, $2p$ excitation, shows a slight difference in trend between the CC and CCC results. Both sets of CC calculations appear to generate very similar results but seem to produce higher cross sections that

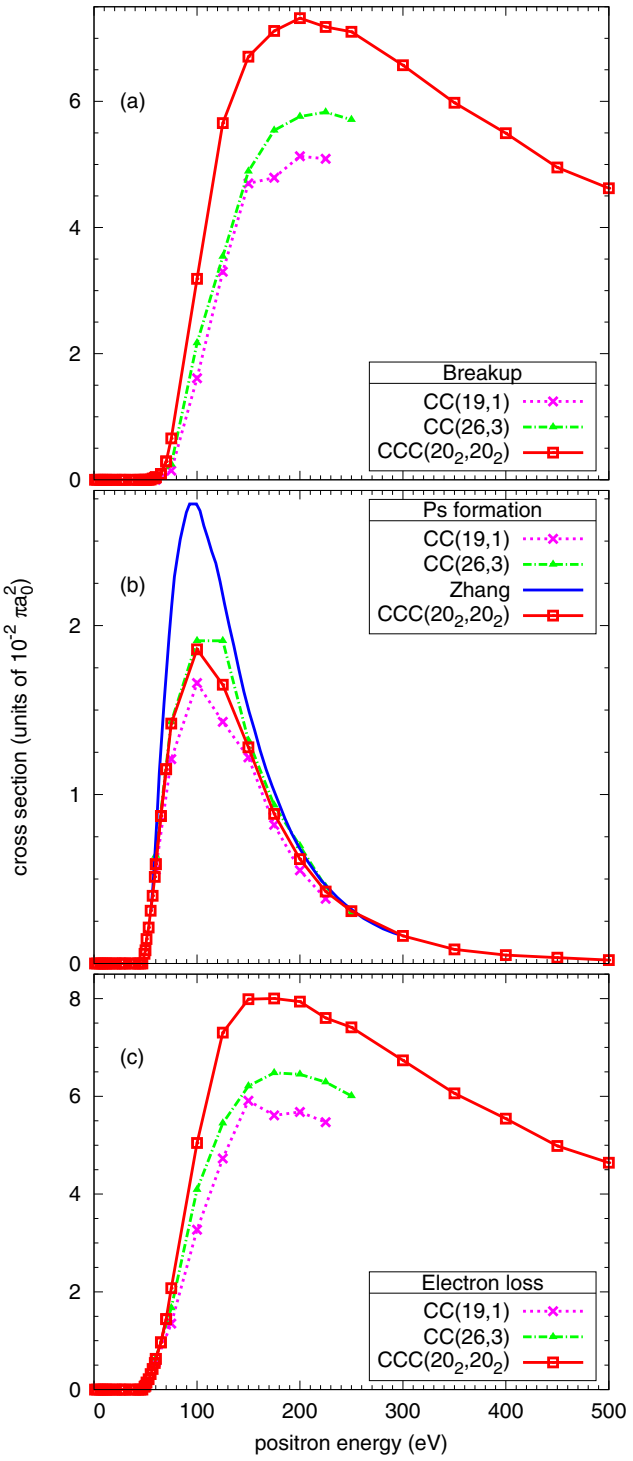

FIG. 8. Breakup (a), Ps-formation (b) and electron-loss (c) cross sections for e^+-He$^+$ scattering. Close-coupling results are from Bransden *et al.* [8] and Ps-formation results are from Zhang *et al.* [10].

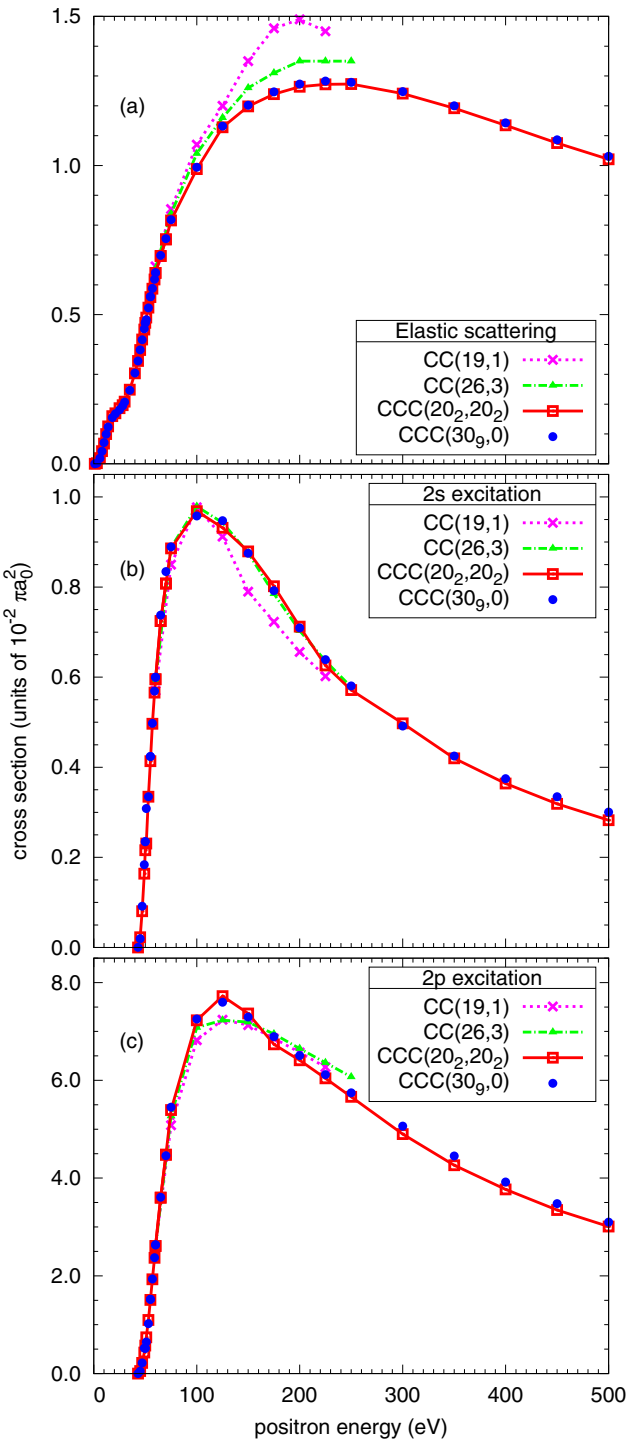

FIG. 9. Cross sections for elastic-scattering (a), 2*s* (b), and 2*p* (c) excitation in e^+-He$^+$ scattering. Close-coupling results are from Bransden *et al.* [8].

the CCC calculations for increasing energy. For each process, single-center CCC results are also presented; the agreement between these results and the two-center CCC results provides further validation via internal consistency checks.

Figure 10 shows the cross sections for Ps formation in the 1*s*, 2*s*, and 2*p* state. The Ps(1*s*) formation cross section resulting from the CCC calculations sits between both sets of CC results. The EPS-CDW results appear much higher than both CC and CCC ones near the peak at 100 eV but become comparable around 200 eV. For Ps(2*s*) formation, the EPS-CDW results are more than double those of the CCC results at the peak. The CC results appear to fluctuate between agreeing with CCC to agreeing with EPS-CDW displaying some unusual behavior.

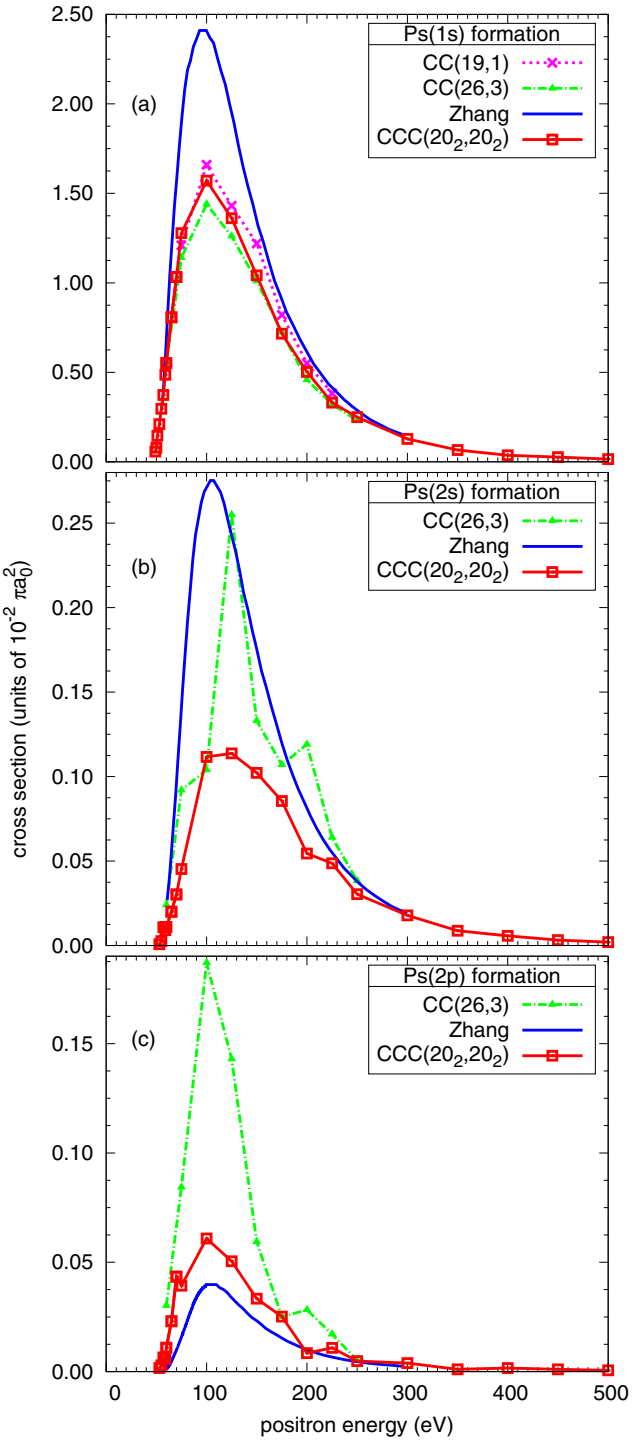

FIG. 10. Cross sections for positronium formation in the $1s$ (a), $2s$ (b), and $2p$ (c) states in e^+-He$^+$ scattering. Close-coupling results are from Bransden *et al.* [8] and Ps-formation results are from Zhang *et al.* [10].

For Ps($2p$) formation, the CCC results are much larger than the EPS-CDW results but significantly smaller than the CC results. Some unphysical deviations can be seen in the CCC-calculated Ps($2s$) and Ps($2p$) cross sections. These arise from numerical instabilities in this highly ill-conditioned system, which are difficult to remove for small cross sections. The analytic treatment of Green's function in the CCC method [34,35] has proven to be very successful in smoothing these points for e^+-H and e^--He$^+$ scattering. Similar improvements would be expected for e^+-He$^+$ scattering, but this is for further investigation. However, due to the overall small size of the Ps($2s$) and Ps($2p$) cross sections in comparison to the grand total and electron-loss cross sections, these numerical instabilities do not affect the internal consistency checks presented in this work.

V. CONCLUSION

The positron-helium ion scattering problem has been studied using the full two-center CCC formalism. The approach to solving this problem is broadly similar to that used for the positron-hydrogen scattering problem. The main exception is the implementation of the momentum-space Coulomb wave function and its corresponding form factor.

Generally, there is some good agreement between the results of previous calculations and the presented CCC calculations, particularly for the larger cross sections. There are some notable exceptions for the total breakup and Ps formation in excited states. Without experimental validation it is difficult to confirm the accuracy of the calculations, but the one- and two-center internal consistency checks give us confidence in the CCC results.

We intend to extend the CCC approach to positron collisions with other hydrogen-like and helium-like ions, one of particular interest being hydride (H$^-$). The reverse of this process is equivalent to antihydride ($\bar{\text{H}}^+$) formation via Ps scattering on $\bar{\text{H}}$ [36]. This is considered to be an important step in antimatter studies since $\bar{\text{H}}^+$ is easier to cool and trap than $\bar{\text{H}}$, meaning that experiments studying the behavior of antimatter in a gravitational field would be easier to perform [37]. Note that two-center approaches to positron scattering are necessary if the reverse process of Ps scattering on the residual ion is of interest. Though not discussed here, the currently developed CCC method may now be applied to Ps scattering on α particles.

ACKNOWLEDGMENTS

The work was supported by the Australian Research Council. We are grateful for access to the Australian National Computing Infrastructure Facility and the Pawsey Supercomputing Centre in Western Australia.

[1] A. S. Kadyrov and I. Bray, J. Phys. B **49**, 222002 (2016).
[2] I. Bray, Phys. Rev. A **49**, 1066 (1994).
[3] I. Bray and A. T. Stelbovics, Phys. Rev. A **46**, 6995 (1992).
[4] A. S. Kadyrov and I. Bray, Phys. Rev. A **66**, 012710 (2002).
[5] T. T. Gien, J. Phys. B **34**, L535 (2001).
[6] S. A. Novikov, M. W. J. Bromley, and J. Mitroy, Phys. Rev. A **69**, 052702 (2004).
[7] B. H. Bransden and C. J. Noble, J. Phys. B **32**, 1305 (1999).
[8] B. H. Bransden, C. J. Noble, and R. J. Whitehead, J. Phys. B **34**, 2267 (2001).

[9] L. Jiao, Y. Wang, and Y. Zhou, J. Phys. B **45**, 085204 (2012).
[10] Y. Z. Zhang, R. M. Yu, S. X. Li, X. D. Song, and L. G. Jiao, J. Phys. B **48**, 175206 (2015).
[11] A. S. Kadyrov and I. Bray, J. Phys. B **33**, L635 (2000).
[12] A. S. Kadyrov, A. V. Lugovskoy, R. Utamuratov, and I. Bray, Phys. Rev. A **87**, 060701 (2013).
[13] I. I. Fabrikant, A. W. Bray, A. S. Kadyrov, and I. Bray, Phys. Rev. A **94**, 012701 (2016).
[14] M. Charlton, A. S. Kadyrov, and I. Bray, Phys. Rev. A **94**, 032701 (2016).
[15] A. S. Kadyrov, C. M. Rawlins, A. T. Stelbovics, I. Bray, and M. Charlton, Phys. Rev. Lett. **114**, 183201 (2015).
[16] C. M. Rawlins, A. S. Kadyrov, A. T. Stelbovics, I. Bray, and M. Charlton, Phys. Rev. A **93**, 012709 (2016).
[17] A. S. Kadyrov, I. Bray, M. Charlton, and I. I. Fabrikant, Nat. Commun. **8**, 1544 (2017).
[18] R. Utamuratov, A. S. Kadyrov, D. V. Fursa, and I. Bray, J. Phys. B **43**, 031001 (2010).
[19] R. Utamuratov, A. S. Kadyrov, D. V. Fursa, I. Bray, and A. T. Stelbovics, J. Phys. B **43**, 125203 (2010).
[20] R. Utamuratov, A. S. Kadyrov, D. V. Fursa, I. Bray, and A. T. Stelbovics, Phys. Rev. A **82**, 042705 (2010).
[21] R. Utamuratov, D. V. Fursa, A. S. Kadyrov, A. V. Lugovskoy, J. S. Savage, and I. Bray, Phys. Rev. A **86**, 062702 (2012).
[22] A. V. Lugovskoy, A. S. Kadyrov, I. Bray, and A. T. Stelbovics, Phys. Rev. A **82**, 062708 (2010).
[23] A. V. Lugovskoy, A. S. Kadyrov, I. Bray, and A. T. Stelbovics, Phys. Rev. A **85**, 034701 (2012).
[24] A. V. Lugovskoy, R. Utamuratov, A. S. Kadyrov, A. T. Stelbovics, and I. Bray, Phys. Rev. A **87**, 042708 (2013).
[25] R. Utamuratov, A. S. Kadyrov, D. V. Fursa, M. C. Zammit, and I. Bray, Phys. Rev. A **92**, 032707 (2015).
[26] C. M. Rawlins, A. S. Kadyrov, and I. Bray, [Eur. Phys. J. D (to be published)].
[27] I. Bray, I. E. McCarthy, J. Wigley, and A. T. Stelbovics, J. Phys. B **26**, L831 (1993).
[28] I. Bray, J. Phys. B **28**, L247 (1995).
[29] I. Bray, J. J. Bailey, D. V. Fursa, A. S. Kadyrov, and R. Utamuratov, Eur. Phys. J. D **70**, 1 (2016).
[30] J. J. Bailey, A. S. Kadyrov, and I. Bray, Phys. Rev. A **91**, 012712 (2015).
[31] I. H. Sloan and E. J. Moore, J. Phys. B **1**, 414 (1968).
[32] V. Eremenko, N. Upadhyay, I. Thompson, C. Elster, F. Nunes, G. Arbanas, J. Escher, and L. Hlophe, Comput. Phys. Commun. **187**, 195 (2015).
[33] J. Mitroy, Aust. J. Phys. **46**, 751 (1993).
[34] A. W. Bray, I. B. Abdurakhmanov, A. S. Kadyrov, D. V. Fursa, and I. Bray, Comput. Phys. Commun. **203**, 147 (2016).
[35] A. W. Bray, I. B. Abdurakhmanov, A. S. Kadyrov, D. V. Fursa, and I. Bray, Comput. Phys. Commun. **212**, 55 (2017).
[36] M. Charlton and D. P. Van Der Werf, Sci. Prog. **98**, 34 (2015).
[37] J. Walz and T. W. Hänsch, Gen. Relativ. Gravit. **36**, 561 (2004).